SUPPLEMENTARY DATA

1-SUPPLEMENTARY MATERIAL AND METHODS

1.1-CELL LINES AND PRIMARY NEUROBLAST CULTURES

HEK 293T cells were used to express the TBCCD1 tagged proteins because they present high transfection efficiency with plasmids. hTERT-RPE-1 cells were used in the majority of this study because they are normal cells immortalized by the stable expression of human telomerase, which can easily differentiate primary cilia. Additionally they are larger and flatter than HEK293T which allows a better visualization of the centrosome, the microtubule cytoskeleton and mitotic spindles. HeLa cells are tumor derived and were essentially used to investigate if there were differences in TBCCD1 localization in different cell types. Mixed primary cell cultures obtained from two-day-old murine dissociated cerebella obtained as described by Lopez-Fanarraga et al (1999) were used to investigate TBCCD1 localization in cells presenting motor cilia. The animals employed in this study were sacrificed following PHS policy and NIH guide.

1.2-RT-PCR EXPRESSION ANALYSIS

The RT-PCR procedure was adapted from Meadus (2003). The amount of cDNA in each sample was first normalized after non-saturing PCR for *hprt* (hypoxanthine guanine phosphoribosyl transferase 1-standard internal control) transcripts. Semi-quantitative RT-PCR expression analysis was performed using the following forward and reverse primers:

	Primer Sequence
Human *hprt* Forward Primer* NM_000194	5´-GGCGTCGTGATTAGTGATG-3´
Human *hprt* Reverse Primer*	5´-CATTACAATAGCTCTTCAGTC-3´
Human/mouse *tbccd1* Forward Primer Hs-NM_018138	5'-CCAGACAGTAACTTTTGCCC-3'
Human/mouse *tbccd1* Reverse Primer	5'-CTCCTTCACAGTTTTCTGCC-3'
Human *rp2* Forward Primer NG_009107.1	5'-GCTGTGGTTCAGGACTATG-3´
Human *rp2* Reverse Primer	5'-AGAAGCTGTCTACATCTCCAG-3´
Human *tbcc* Forward Primer NM_003192.2	5'-TGACCGAACTGAGCAAC-3'
Human *tbcc* Reverse Primer	5'-CCACTGGATATTTCGCTC-3'

* Nolasco et al, 2005

1.3-siRNA SEQUENCES

The following TBCCD1 specific siRNA duplexes were used:

A-Purchased from Dharmacon

5´-GUGGCUUUACUUCGAAAUA-3´

B-Purchased from Ambion

5´-GAGCUAAGAUUGCUUGUAA-3´

5´-GAUUCAUCGUUGCAACGAA-3´

5´-CCUUGUGAAUUCUAUGUAU-3´

1.4-COMMERCIAL AND OFFERED ANTIBODIES

Commercially available antibodies used: anti-GFP (A11122) and anti-golgin97 (Molecular Probes); anti-α-tubulin (DM1A and B512), anti-β-tubulin (TUB2.1), anti-γ-tubulin (GTU88), anti-δ-tubulin (DTU-64) and anti-β-Actin conjugated to peroxidase (AC-15) are from Sigma. Anti-polyglutamylated tubulin (GT335) and anti-IFT88/polaris were kind gifts from Janke C and Dedouets C, respectively. Secondary antibodies used: anti-mouse (Alexa 488), anti-rabbit (Alexa 594), anti-rabbit (Alexa 350) from Molecular Probes and Cy3-conjugated goat antimouse IgG1 from Jackson Immunoresearch.

In the experiments requiring immunostaining with two primary antibodies produced in mouse the incubation was performed sequentially. First the cells were incubated with the anti-TBCCD1 serum, followed by incubation with anti-mouse Alexa488. After extensive washing, the cells were incubated with anti-golgin97 (IgG1) or with anti-poly-glutamylated tubulin and finally with the anti-mouse IgG1 antibody.

1.5-COMPLEMENTATION ASSAY IN *S. cerevisiae*

The functional complementation assay in yeast was performed as described by Bartolini et al, 2002. The wild-type (MATa; his3D1; leu2D0; lys2D0; ura3D0) and a ΔCIN2 (Mat a; his3D1; leu2D0; lys2D0; ura3D0; YPL241c::kanMX4) strains obtained from Euroscarf were transformed with empty pRS413 or pRS413-TBCCD1. Cells transformed with pRS413-CIN2 (kind gift from F Bartolini and NJ Cowan; Bartolini et al, 2002) and pRS413-TBCC were used as positive controls. Transformants were

selected and single colonies were picked and grown overnight at 30ºC in liquid medium without the appropriate amino acids. Transformants were re-suspended in sterile water at the same optical density. Serial dilutions of cell suspensions were spotted in yeast extract/peptone/dextrose (YPD) medium with 0, 1, or 5 µg/ml of benomyl. A YPD plate supplemented with DMSO was also used as control growth conditions because benomyl was dissolved in DMSO. The cells were grown at 26ºC.

1.6-STATISTICAL ANALYSIS

Differences between the data were tested for statistical significance by t-test. P values less than 0.05 were considered statistically significant

Fig. Supl.1A

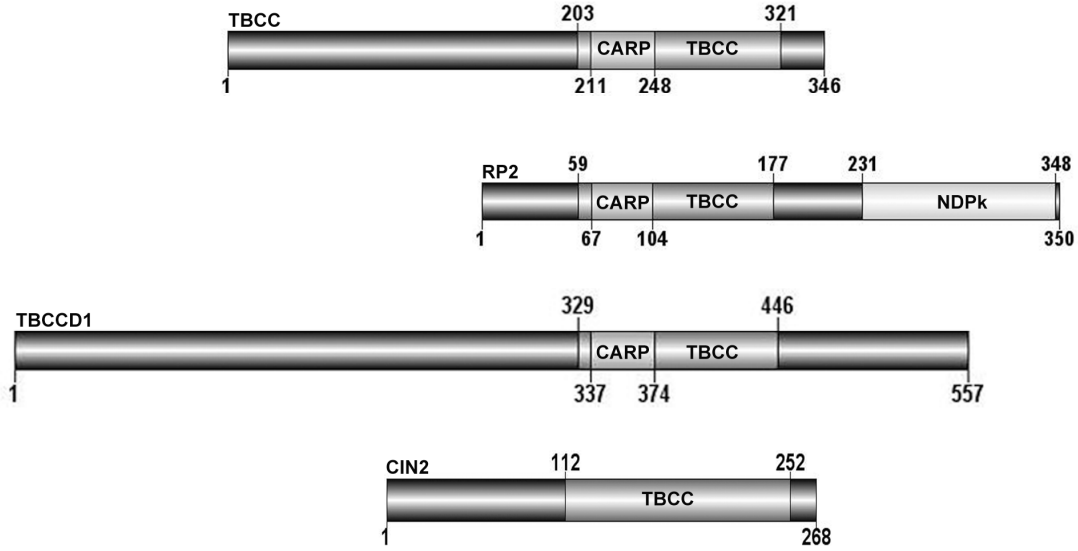

Fig. Supl. 1B

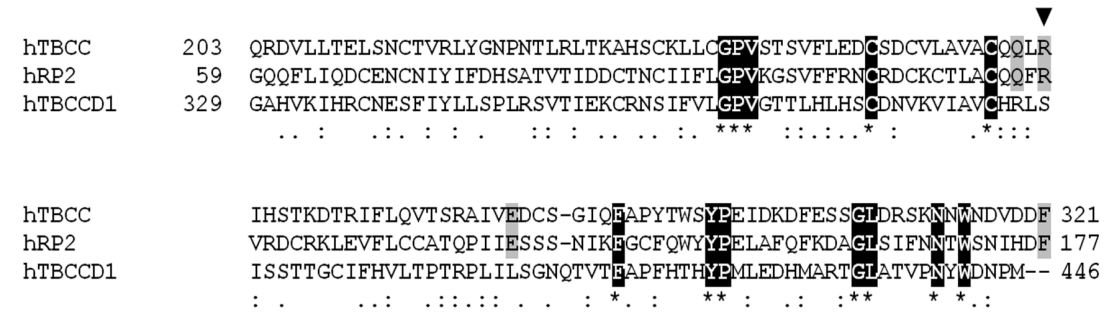

Fig. Supl. 1C

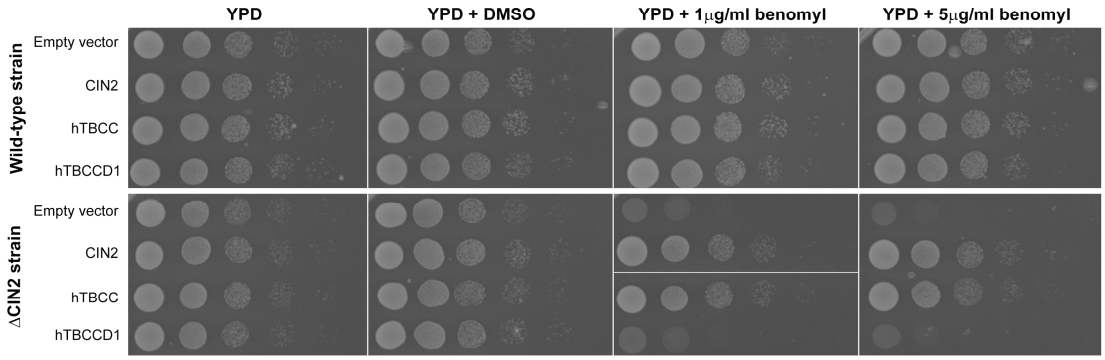

Fig S1- TBCCD1 does not complement CIN2 deletion in yeast.

(**A**) Schematic representation of the functional domains ascribed to human TBCC, RP2 and TBCCD1 and yeast CIN2. The human proteins also possess a CARP domain (Freeman et al., 2000) (**B**) Sequence alignment of the TBCC domains of TBCC, RP2 and TBCCD1. A comparison between the putative TBCCD1 aminoacid sequence and human TBCC and RP2 only revealed a 13.6% and 8.7% identity, respectively. These values increase to 21.1% and 26.7%, respectively, at the TBCC domain. Highlighted in grey are the amino acid residues conserved in TBCC and RP2 that are important for the catalytic activity of RP2. Highlighted in black are the amino acid residues conserved between the three proteins. The arrowhead marks the conserved arginine crucial for the GAP activity of TBCC and RP2 towards tubulin. (**C**) Yeast complementation assay. The deletion of yeast TBCC (CIN2) causes hypersensitivity to cold and to the MT depolymerising agent benomyl. A wild-type strain and a ΔCIN2 strain were transformed with an empty vector or a plasmid expressing CIN2, human TBCC or human TBCCD1

and the resulting strains were assayed for their resistance to benomyl. As expected, the plasmids carrying CIN2 or human TBCC could rescue the phenotype. However, TBCCD1 did not complement the loss of CIN2.

Fig. Supl. 2A

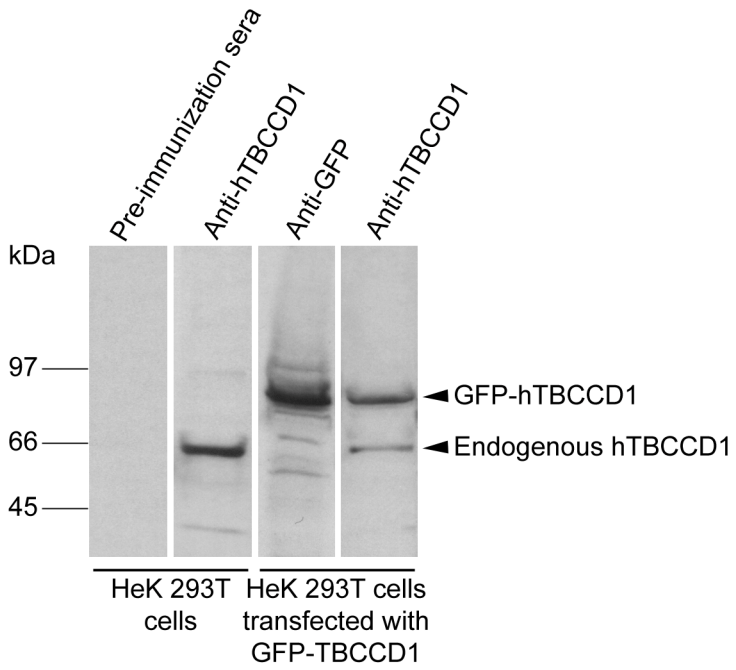

Fig. Supl. 2B

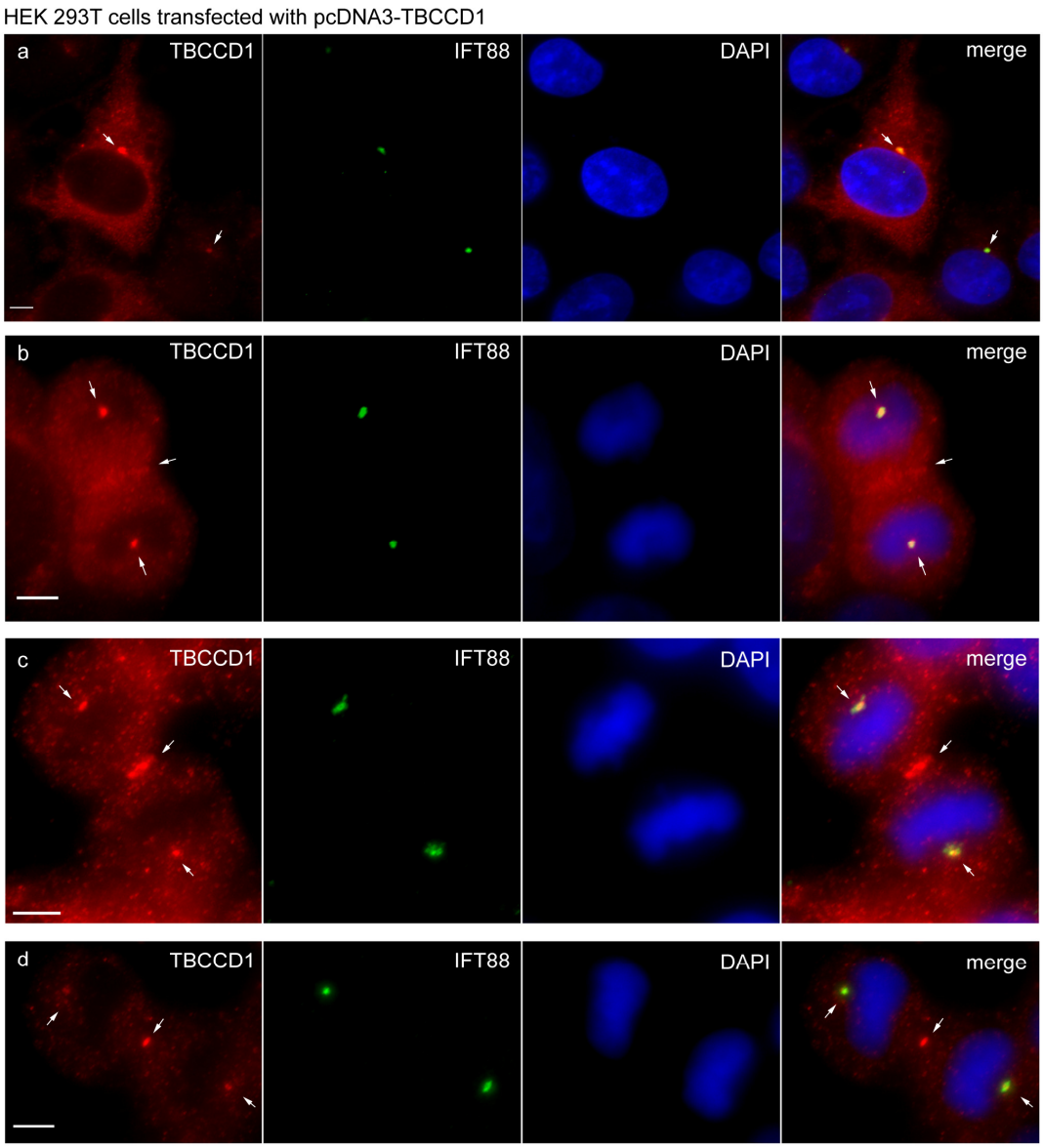

Fig S2 - TBCCD1 polyclonal antiserum production.

(**A**) Protein extracts from Hek 293T non transfected cells or transfected with a plasmid containing GFP-TBCCD1 were analysed by 10% SDS-PAGE followed by Western blot. The extracts of non transfected cells were incubated with pre-immunization serum or with anti-TBCCD1. The extracts of GFP-TBCCD1 transfected cells were incubated with an anti-GFP antibody or anti-TBCCD1. (**B**) Hek 293T cells were transfected with a plasmid containing untagged-TBCCD1 (pcDNA3-TBCCD1) and immunostained using antibodies against TBCCD1 and IFT88 (**a**) interphase cell, (**b,c**) mitotic cells (**d**) cytokinesis. DNA was stained with DAPI. Scale bars = 5µm. The different levels of untagged-TBCCD1 are discriminated by the antibody against TBCCD1 (see panel **a**).

Arrows point to TBCCD1 localization at the centrosomes, spindle midzones and midbody.

Fig. Supl. 3A

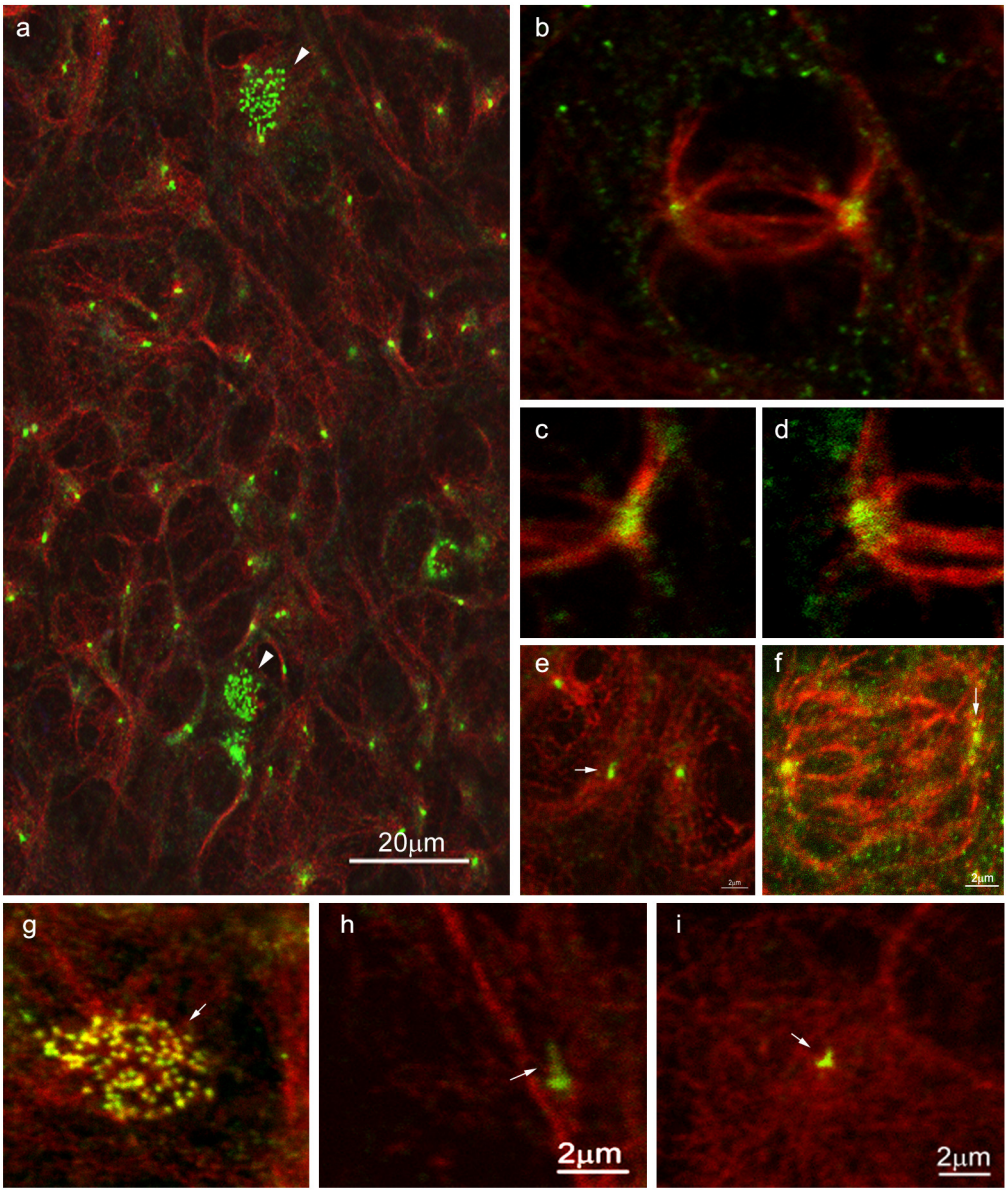

Fig. Supl. 3B

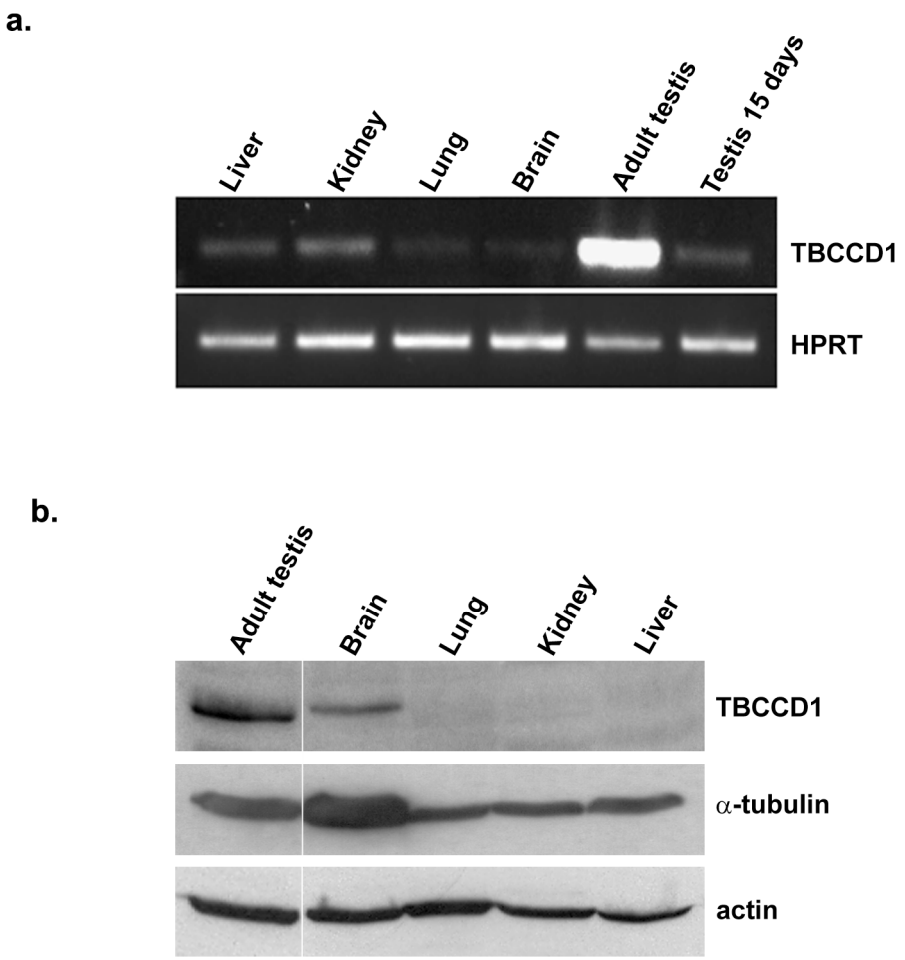

Fig S3- Sub-cellular localization of TBCCD1 in primary mouse neuroblast cultures and *tbccd1* expression analysis in different mouse tissues.

(**A**) Immunostaining of mixed primary cell cultures obtained from two-day-old murine dissociated cerebella with anti-TBCCD1 and anti-α-tubulin showing its centrosome/basal body localization. Arrows point to TBCCD1 at centrosomes and basal bodies of motile cilia. Note the localization of TBCCD1 in the spindle poles (**b-d** and **f**). (**B**) *Tbccd1* expression analysis in mouse tissues. Semi-quantitative RT-PCR analysis was performed with specific *Tbccd*1 primers, common to the mouse and human transcripts. *Hprt* (hypoxanthine guanine phosphoribosyl transferase 1) expression was used as an internal control (**a**). Western blot analysis of mouse tissues protein extracts performed with the anti-TBCCD1 serum and with antibodies against α-tubulin and actin (**b**).

Fig. Supl. 4

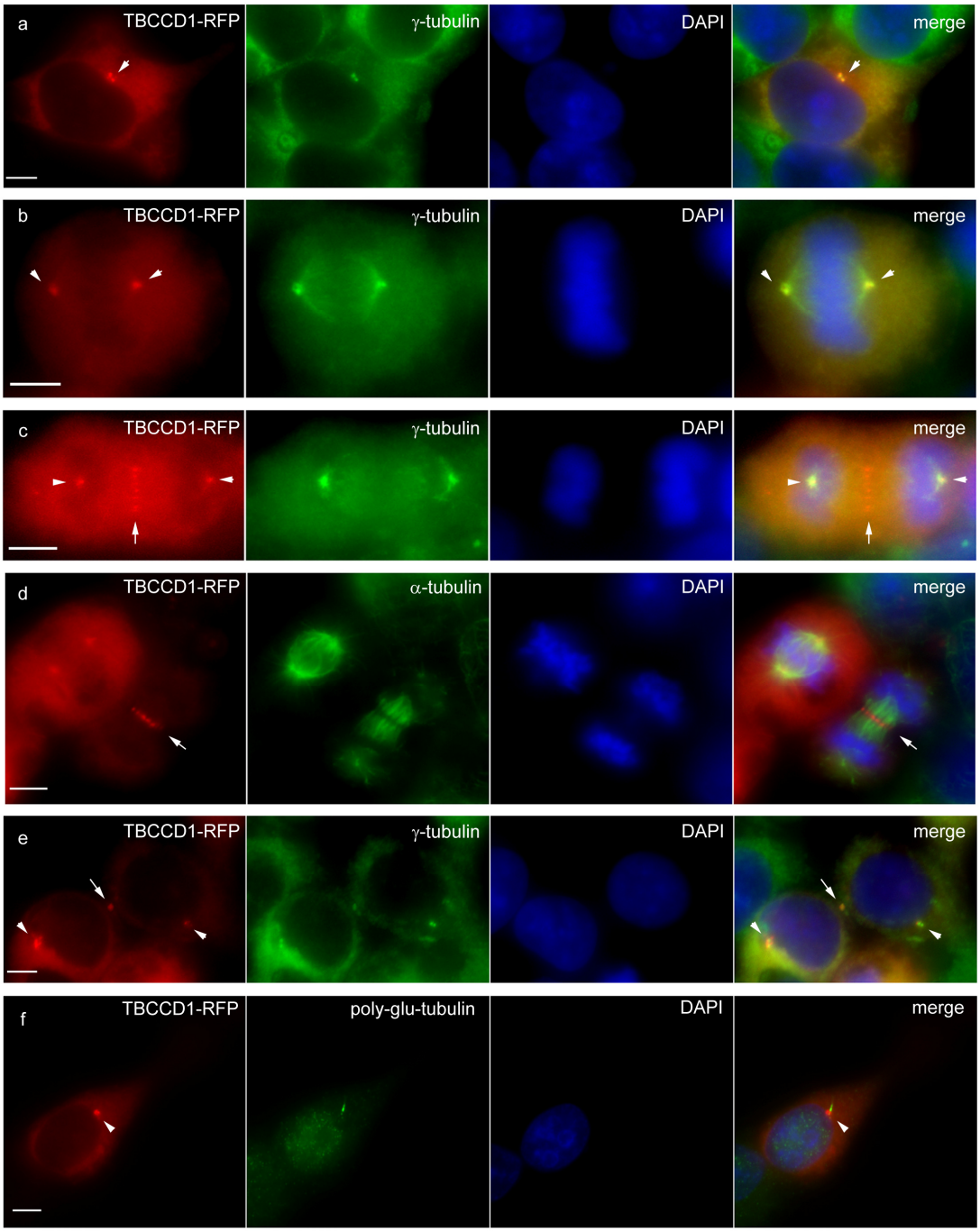

Fig S4- Sub-Cellular localization of TBCCD1-RFP in Hek 293T cells

Hek 293T cells were transfected with a plasmid containing TBCCD1-RFP and immunostained using antibodies against γ-tubulin **(a-c and e)**, α-tubulin **(d)** or poly-glutamylated tubulin **(f).** DNA was stained with DAPI. **(a)** Interphase cell; **(b and d)** Cell in methafase; **(c and d)** Cell in anaphase; **(e)** Cell in cytokinesis; **(f)** Cell cycle arrested cell after serum starvation for 24 h showing a primary cilium. Arrowheads

point to TBCCD1-RFP at centrosomes **(a-c, e)** and basal body **(f)**. Arrows indicate the spindle midzone **(c and d)** and midbody **(e)**. The same analysis was performed by expressing GFP tagged TBCCD1 either at the C- or N-terminal regions being the results the same as for TBCCD1-RFP. Scale bars = 5μm.

Fig. Supl. 5A

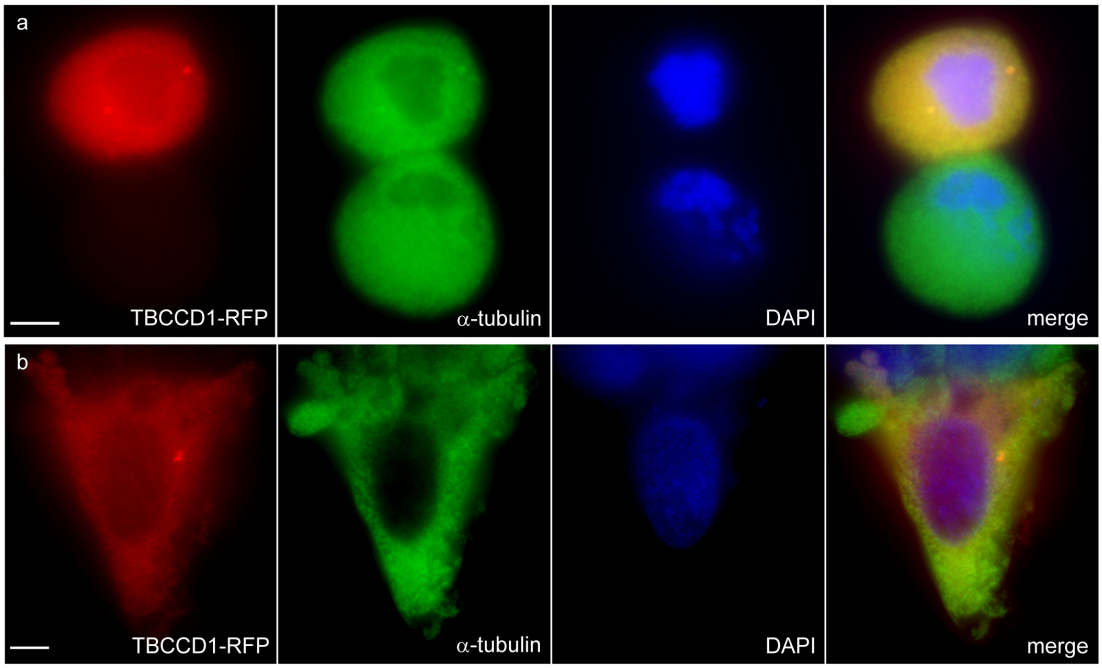

Fig. Supl. 5B

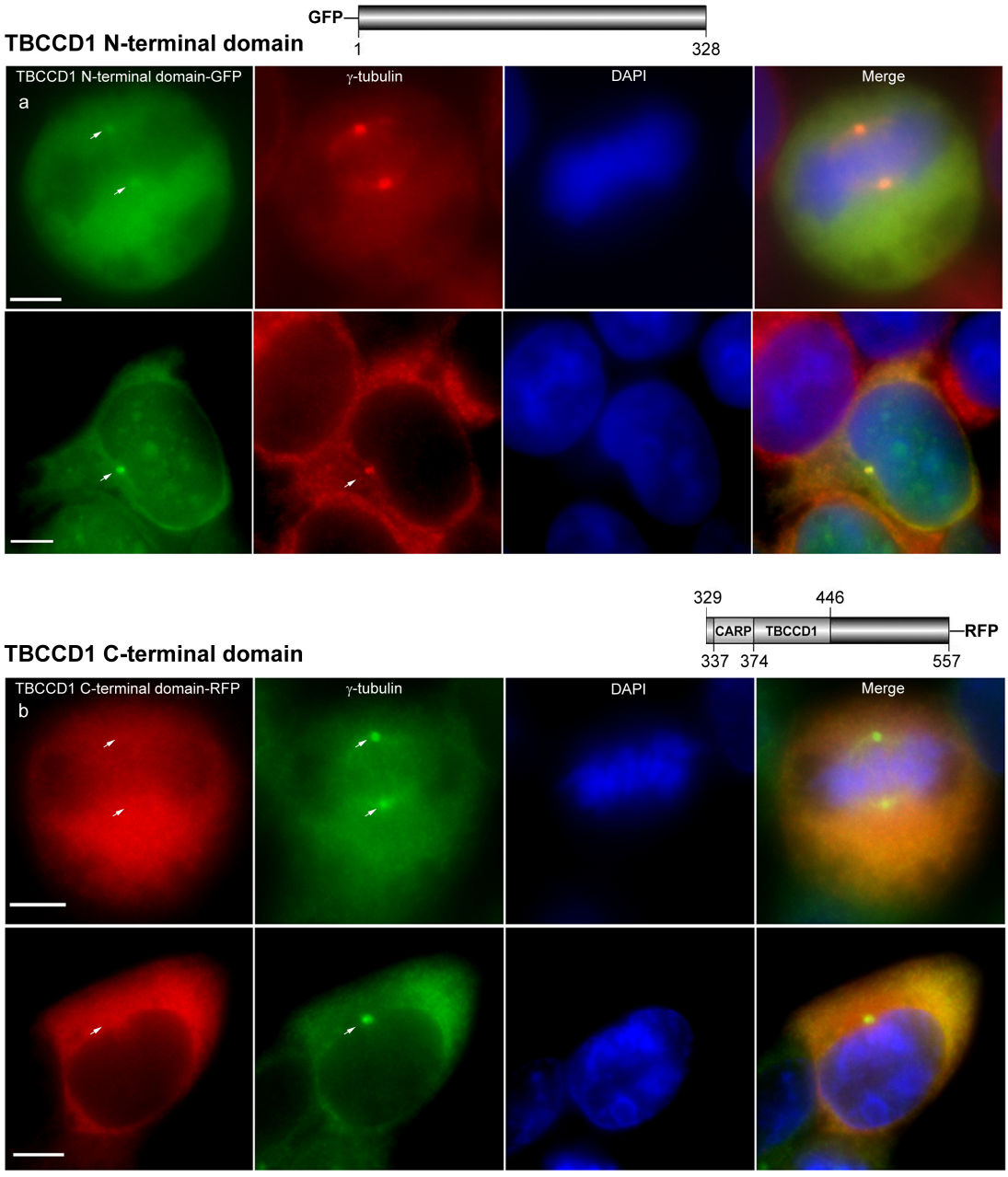

Fig S5- TBCCD1 localization in centrosomes is independent of microtubules and requires the N-terminal domain of the protein.

(**A**) Hek 293T cells transfected with a plasmid carrying TBCCD1-RFP were treated with nocodazole for 1 hour and were stained with γ-tubulin antibody. The fusion protein was observed at the centrosome in mitotic (**a**) and interphase (**b**) cells. (**B**) **(a)** Mitotic and interphase cells expressing TBCCD1 N-terminal domain-GFP. (**b**) Mitotic and interphase cell expressing TBCCD1 C-terminal domain-RFP with the TBCC and CARP domains. The TBCCD1 C-terminal region (329-557aa), containing the TBCC and

CARP domains, does not localize to the centrosome (**b**), whereas the N-terminal domain (1-328aa) seems to be sufficient for its centrosomal localization (**a**). Arrows point to the presence **(a)** or the absence **(b)** of the truncated tagged proteins at centrosomes. Scale bars = 5µm.

Fig. Supl. 6A

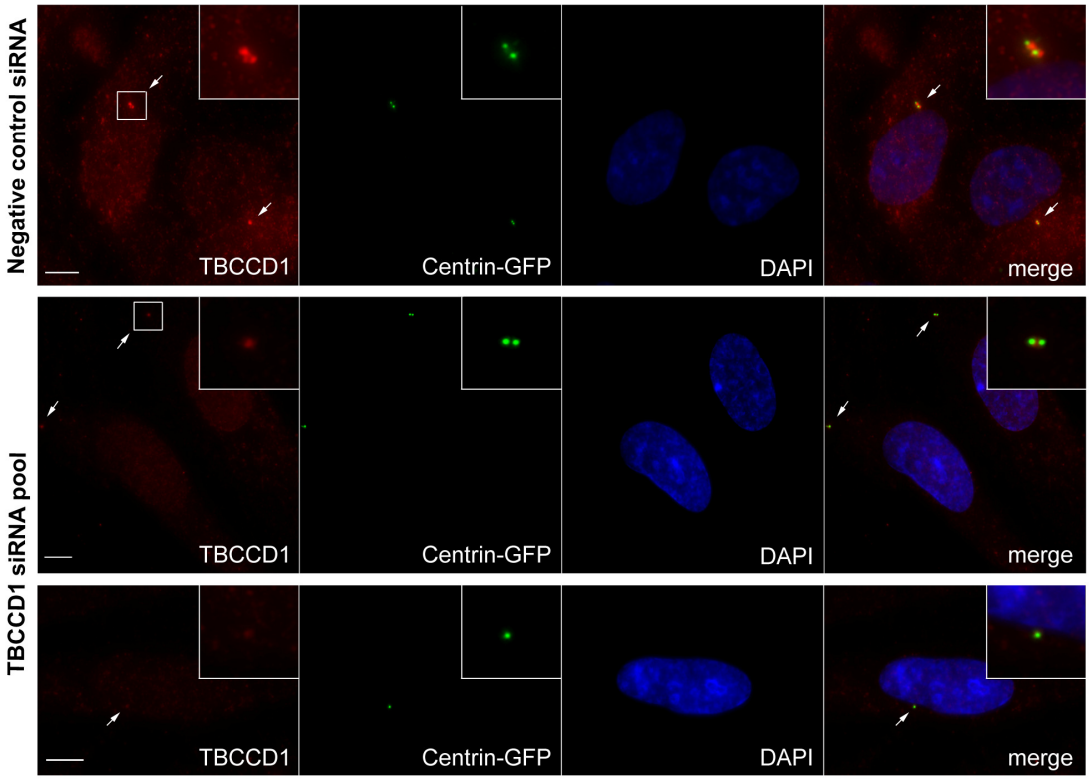

Fig. Supl.6B

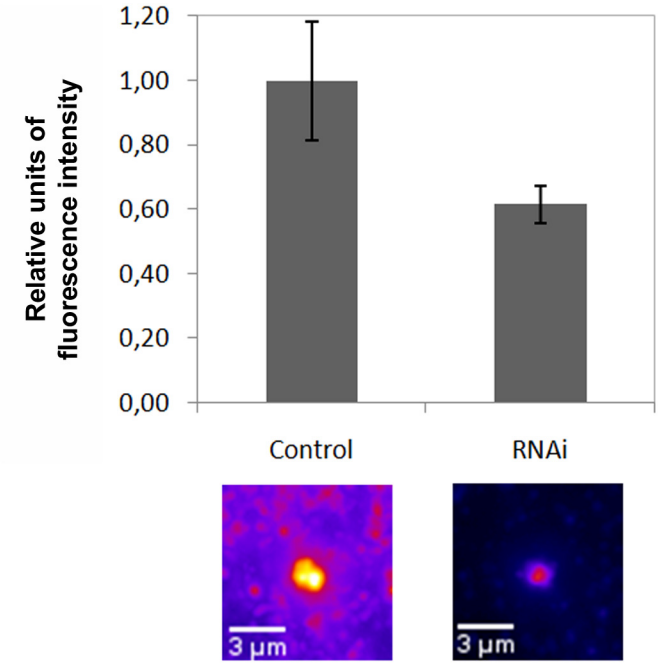

Fig. Supl. 6C

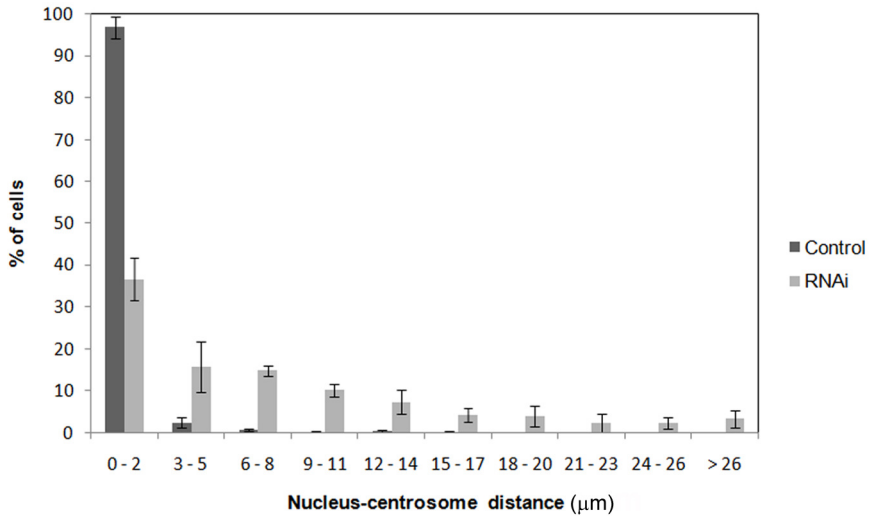

Fig. Supl. 6D

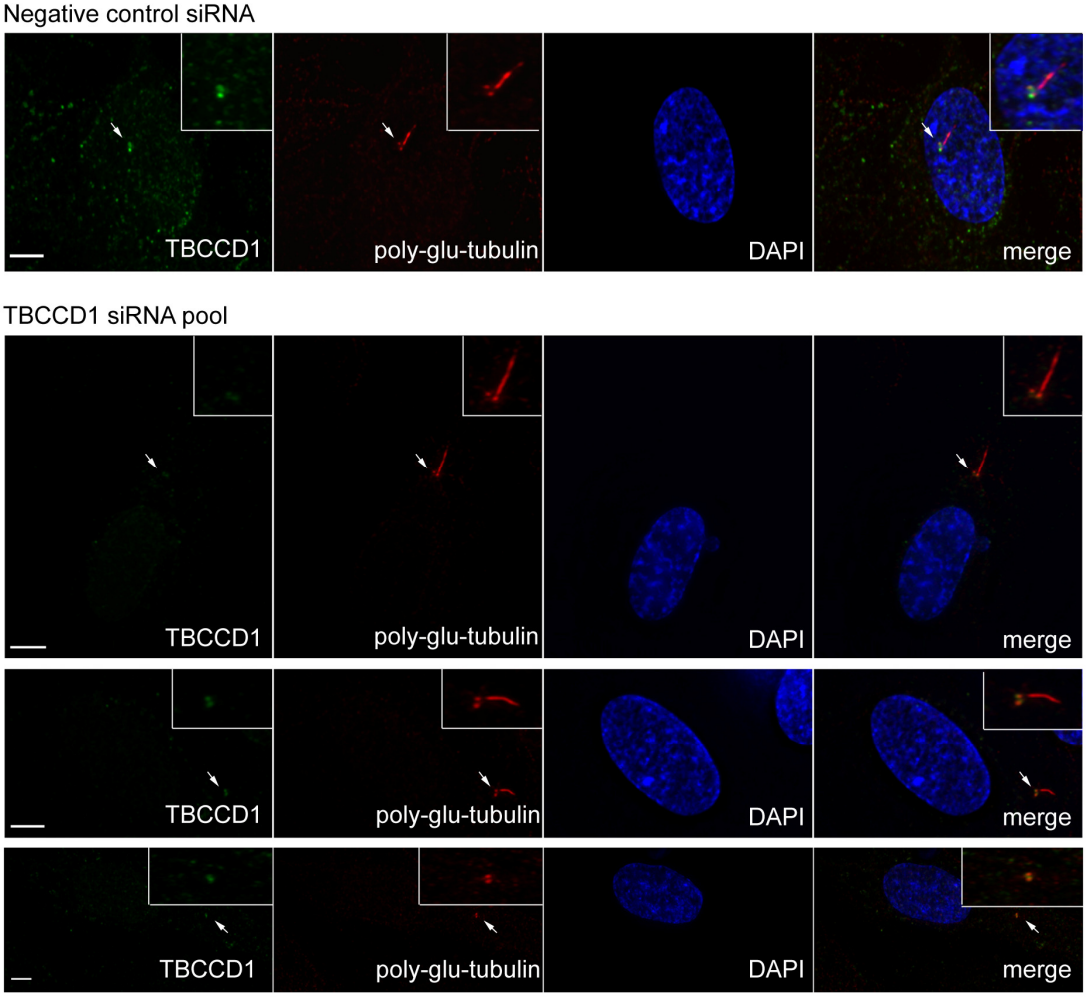

Fig. Supl. 6E

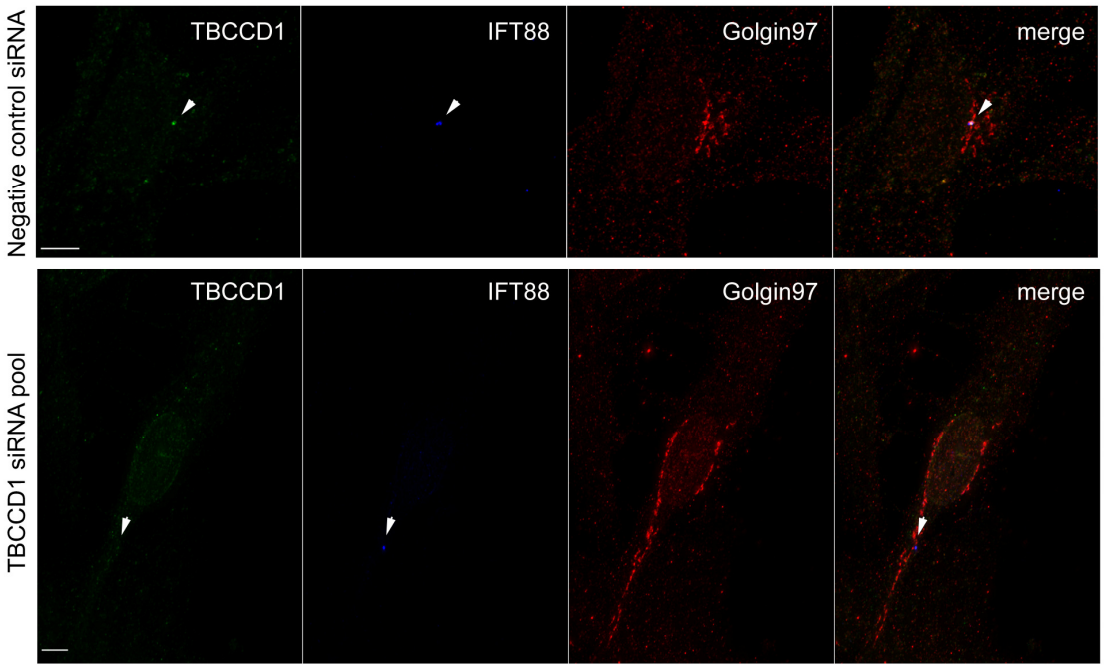

Fig S6- Immunofluorescence analysis of TBCCD1 silencing in RPE-1 cells

(**A**) RPE-1 centrin-GFP control (upper panel) and TBCCD1 siRNA pool treated cells (lower panels) were immunostained with the anti-TBCCD1 serum. Details show enlarged images of centrosomes. Scale bar =10μm **(B)** Fluorescence intensity at the centrosome was quantified using ImageJ software in images acquired using the same exposure conditions. The graphic shows relative units of fluorescence intensity from control (1±0.18; n=92 cells scored) and RNAi cells (0.62 ± 0.06; n=85 cells scored) which differ significantly ($p<0.001$ as determined by t-test). Representative images of centrosome in a control cell, as well as a centrosome from an RNAi cell that were false coloured to highlight the fluorescence intensity differences, are shown. The difference between the 65% of decrease of the TBCCD1 levels observed by analyzing the proteins extracts of TBCCD1 depleted cells by western blot (Fig 2) and the 40% decrease of the TBCCD1 staining intensity at the centrosome could be due to the contribution of cytoplasmic pool of the protein. **(C)** Histogram showing the distribution of nucleus centrosome distances (mean percentage ± SD) in control (n=826 cells scored) and TBCCD1 silenced cells (n=813 cells scored). **(D)** Control and TBCCD1 RPE-1 depleted cells were induce to form primary cilia and then immunostained with anti-TBCCD1 serum and anti-poly-glutamylated tubulin. In the RNAi cell population we observed cells with and without cilia having centrosomes with similar low TBCCD1 remaining levels. Scale bar =5μm. **(E)** Control and TBCCD1 siRNA pool treated cells immunostained with antibodies against TBCCD1, IFT88 and golgin97. There was no apparent co-localization of the TBCCD1 and Golgi staining. Scale bar =10μm

Fig. Supl. 7A

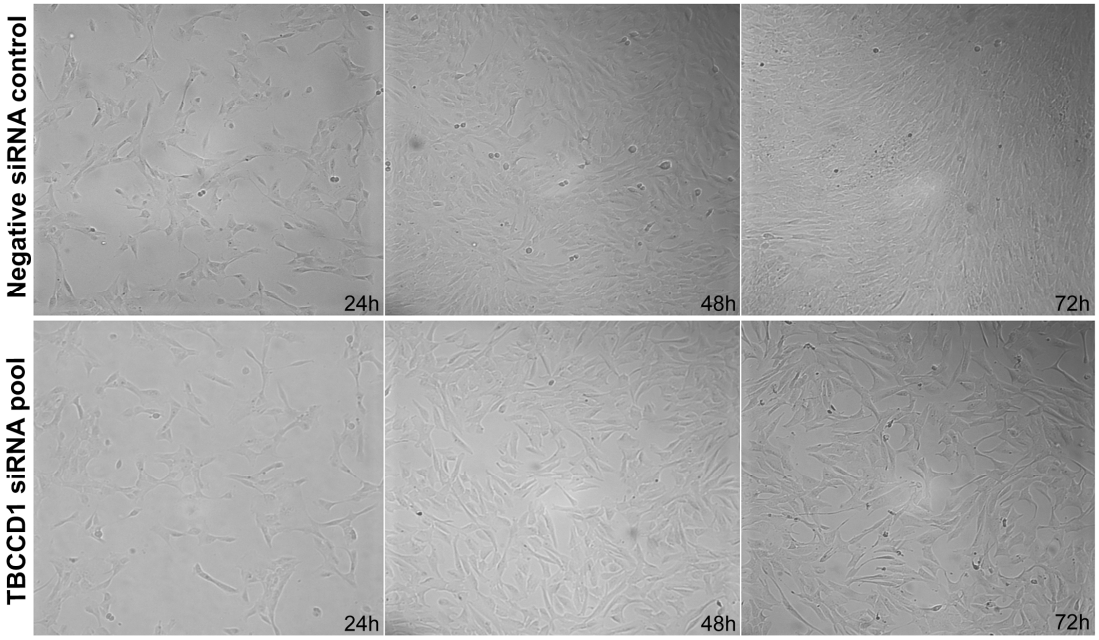

Fig. Supl. 7B

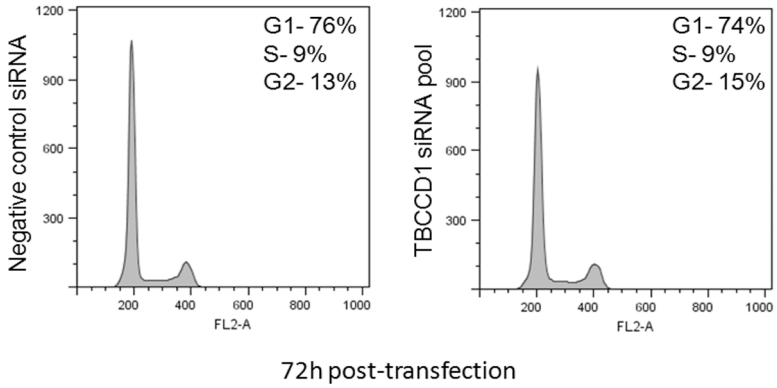

Fig S7- TBCCD1 knockdown by RNAi leads to cell cycle delay in RPE-1 cells. (**A**) RPE-1 control or TBCCD1 silenced cells, were observed by transmitted light microscopy. After 48h and 72h of transfection the cells transfected with the TBCCD1 siRNA pool showed a lower density than those transfected with the negative control siRNA. **(B)** Flow cytometry analysis of control and TBCCD1 depleted cells stained with propidium iodide 72h post transfection. In control cells, an increase in the G1 DNA content population was observed when compared with control cells 48h post-transfection. Accordingly, a decrease in the G2 DNA content population was observed. These observations are probably due to the fact that at 72h post-transfection, control cells are approaching confluence where they are expected to stop dividing. In RNAi cells the percentage of G1 cells does not change

significantly from 48h to 72h post-transfection whereas an increase in the S and G2 populations is observed. This and the fact TBCCD1 silenced cells cells do not reach confluence 72h post-transfection suggests that they may not progress to mitosis.

Fig. Supl. 8

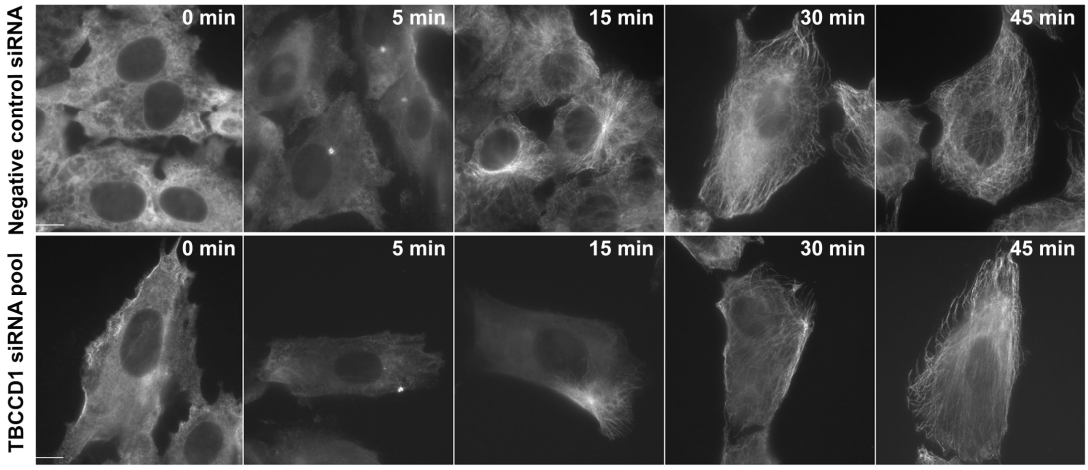

Fig S8- MT regrowth- TBCCD1 is not required for MT nucleation at the centrosome. RPE-1 control and TBCCD1 depleted cells were treated with Nocadozale (30 μM) for 45 min. After nocodazole washout, MT-regrowth was followed for 0, 5, 15, 30 and 45 minutes. At each time point the cells were fixed and subsequently processed for immunofluorescence with an anti-α-tubulin antibody. As in control cells, MTs were still nucleated and anchored at the centrosome. Scale bar = 10 μm.

Fig. Supl. 9

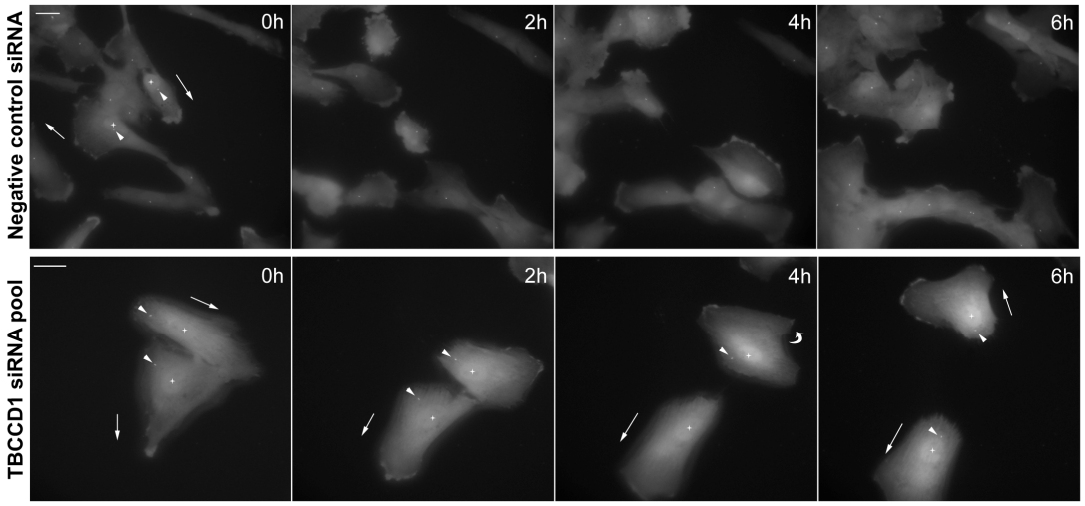

Fig S9- Centrosome positioning in moving TBCCD1 depleted RPE-1 cells.

Centrosome positioning relative to the nucleus during movement was analysed by live imaging of non-confluent RPE-1 centrin-GFP cells. Time points are shown in the upper right corner of each frame. Arrowheads point to the centrosomes and nuclei centers are indicated by asterisks. Arrows indicate the direction and orientation of the movement of each cell. Scale bar = 20 μm

Legend- movies S1 and S2

Control and TBCCD1 silenced RPE-1 centrin-GFP cells were imaged at 2 min interval for 8 h on DeltaVision Core System (Applied Precision) equipped with a climate chamber using a 60X objective (Olympus U-PLlan Apo N, UIS2, 1-U2B933). The movies were assembled using SoftWorx software. In RPE-1 centrin-GFP RNAi cells centrosomes are preferentially localized behind the nucleus and cell movements are slower in comparison with controls. In control cells the centrioles present a dynamic behaviour in which they temporarily slightly distance from each other whereas in TBCCD1 RNAi cells this dynamic seems to be affected.

Legend- movies S3 and S4

Wound-healing progression is slower in RPE-1 RNAi cells. Control and siRNA treated cells were imaged at 4 min time intervals for 9h on a on DeltaVision Core System equipped with a climate chamber using a 20x objective (Olympus U-Plan S-Apo 20x/0.75). The movies were assembled using SoftWorx software.

3- SUPLEMENTARY REFERENCES

Fanarraga ML, Avila J, Zabala JC (1999) Expression of unphosphorylated class III beta-tubulin isotype in neuroepithelial cells demonstrates neuroblast commitment and differentiation. *Eur J Neurosci* **11**:517-527

Freeman NL, Field J (2000) Mammalian homolog of the yeast cyclase associated protein, CAP/Srv2p, regulates actin filament assembly *Cell Motil Cytoskeleton* **45:**106-120

Nolasco S, Bellido J, Gonçalves J, Zabala JC, Soares H (2005) Tubulin cofactor A gene silencing in mammalian cells induces changes in microtubule cytoskeleton, cell cycle arrest and cell death. *FEBS Lett* **579:**3515-3524

Meadus, WJ (2003) A semi-quantitative RT-PCR method to measure the in vivo effect of dietary conjugated linoleic acid on porcine muscle PPAR gene expression *Bio Proced Online* **5**, 20–28